An electrically-tunable liquid crystal lens coupler for the fiber communication systems

Chyong-Hua Chen*, Michael Chen, Yi-Hsin Lin
Department of Photonics, National Chiao Tung University, 1001 Daxue Rd., Hsinchu 30010, Taiwan
*chyong@mail.nctu.edu.tw

ABSTRACT

In this study, we demonstrated an electrically tunable lens coupler for both variable optical attenuation (VOA) and polarization selection. This coupler consists of a liquid crystal (LC) lens sandwiched between two GRIN lens. A GRIN lens is used to couple the light into the single mode fiber, and a LC lens is used to electrically manipulate the beam size of light. It is known that the lens power of a LC lens is tunable with high polarization sensitivity. Then, as the applied voltage on the LC lens is zero, the incident light is focused due to GRIN lens and coupled into the fiber. On the other hand, the beam size of the transformed e-ray becomes larger because the lens power of a LC lens for the e-ray decreases with the increase of the applied voltage. This results in the decrease of the coupling efficiency, and the optical power coupled into the fiber is smaller. This lens coupler for the e-ray functions as a VOA due to a continuous optical attenuation. On the contrary, the lens power of this LC lens for the o-ray does not vary because of optical anisotropy of the LC layer, and then the coupling efficiency for the o-ray remains high. For an arbitrary polarized incidence, this tunable lens coupler acts as a broadband polarizer for the fiber systems. The polarization dependent loss is larger than 30 dB and the switching time is around 1 second.

Keywords: Liquid Crystal Lens, Lens Coupler, Variable Optical Attenuator, Polarizer

1. INTRODUCTION

The liquid crystal (LC) has been studied for many years, and a lot of related applications emerge in our daily life, such as liquid crystal displays. Due to its uniaxial optical property, the LC becomes a promising candidate for various photonic applications in which the phase shift, phase retardation as well as amplitude of light wave come into play. Moreover, the tunable birefringence of the LC via the external electric fields makes it an important role in many kinds of light manipulation, including polarization switching, diffraction of light, and wavefront transformation through the LC-based spatial light modulators. Blooming of photonic devices and growing need provide a great opportunity for the next–generation LC technology, with broader spectrum ranges, i.e. visible, infrared to terahertz, and more degree of freedom as a perspective of optics. So far, numerous LC devices have been simulated, demonstrated, and commercialized, which include several types of bio-sensors [1-3], variable optical attenuators (VOAs) [4-5], LC lenses [6-7], in-line polarizers [8], and Laguerre-Gaussian beam generators [9-10]. Among them, LC lenses have been demonstrated and further improved for various applications, such as imaging systems [11], electrically tunable zoom systems [12], concentrated photovoltaic systems [13], holographic systems [14] and ophthalmic lens [15]. In order to combine the coupling ability

Emerging Liquid Crystal Technologies X, edited by Liang-Chy Chien, Harry J. Coles, Hirotsugu Kikuchi, Ivan I. Smalyukh,
Proc. of SPIE Vol. 9384, 938411 · © 2015 SPIE · CCC code: 0277-786X/15/$18 · doi: 10.1117/12.2081973

of lens couplers and the optical power adjustment capability of VOAs, we previously proposed an electrically tunable lens coupler consisting of an LC lens and demonstrated through a multimode fiber [16]. The coupling efficiency was up to 0.8 and the tunable attenuation range was around 15 dB. In addition, we also utilized the polarization sensitivity of the tunable lens coupler to achieve an electrically tunable linear polarizer for fiber systems [17]. Because of the negligible dispersion of the LC, the polarization dependent loss can be up to 12 dB from visible to near infrared range. However, these might be useful for bio-sensor devices but not so practical for fiber communication systems, because the aforementioned tunable lens could only be applied in multimode fiber systems. Therefore, realizing an electrically tunable lens coupler acted as a lens coupler for a wide spectrum range to continuously adjust the transmitted optical power and to provide good selectivity of polarization for single mode fiber systems becomes our main objective.

In this study, we simulate and demonstrate a broadband and electrically tunable lens coupler for fiber coupling, variable optical attenuation, and polarization selection in a single mode fiber system. To increase the maximum lens power for further reduction of the beam waist impinged on the single mode fiber for the fiber coupling, a gradient refractive index (GRIN) lens is adopted and contacted with the original LC lens. When the lens power is equal to zero, the incident beam of a designed wavelength can be coupled into the fiber. Incident light with distinct wavelength can achieve their maximum coupling efficiency via different lens powers provided by LC lens, which complement the dispersion effect of the GRIN lens. At this moment, the tunable lens coupler has a function of a lens coupler. As for the designed wavelength, the optical power transmitting into the fiber gradually decreases when the lens power of the LC lens increases, where the tunable lens coupler acts as a VOA. Moreover, the incidence can be categorized as an extraordinary ray (e-ray) and an ordinary ray(o-ray) whose electric field are parallel and perpendicular to the alignment direction of the LC layer, respectively. The wavefront of the e-ray varies as the lens power of the LC lens changes while that of the o-ray remains the same. As a result, the o-ray has a high coupling efficiency, and the e-ray experiences an extreme power loss when the LC lens provides a large lens power. This makes the tunable lens coupler become a polarizer for single mode fiber systems. We believe the device proposed in this study creates a new opportunity in fiber communication systems nowadays.

2. SYSTEM STRUCTURE AND OPERATING PRINCIPLES

The LC lens in this experiment is identical with the one presented before for multimode fiber system applications [16]. It comprises of three glass substrates with Indium Tin Oxide (ITO) transparent electrodes, two alignment layers using Polyvinyl Alcohol (PVA), a UV glue (Norland product Inc., NOA81) for insulating layer, and an LC layer (Merck, Δn =0.2609 , 589.3nm). In Fig. 1(a), the thicknesses of insulating layer (d_{IN}), glass substrates (d_G), and LC layer (d_{LC}) are 25μm, 700μm, and 50 μm, respectively. In order to generate an inhomogeneous electric field among the LC layer for producing a nearly parabolic phase distribution for lensing effect, the ITO electrode of the central glass substrate is etched a hole-pattern at the center. The effective aperture of the LC lens is ~1.33mm and its lens power (reciprocal of focal length) range for 633nm wavelength is from -8.9 m^{-1} to 30.3m^{-1} [16]. The tunable range for different wavelength can also be evaluated via Cauchy's equation as we have demonstrated before [16-17]. The LC lens is attached with a GRIN lens and the combination of the two is called tunable lens coupler in this article.

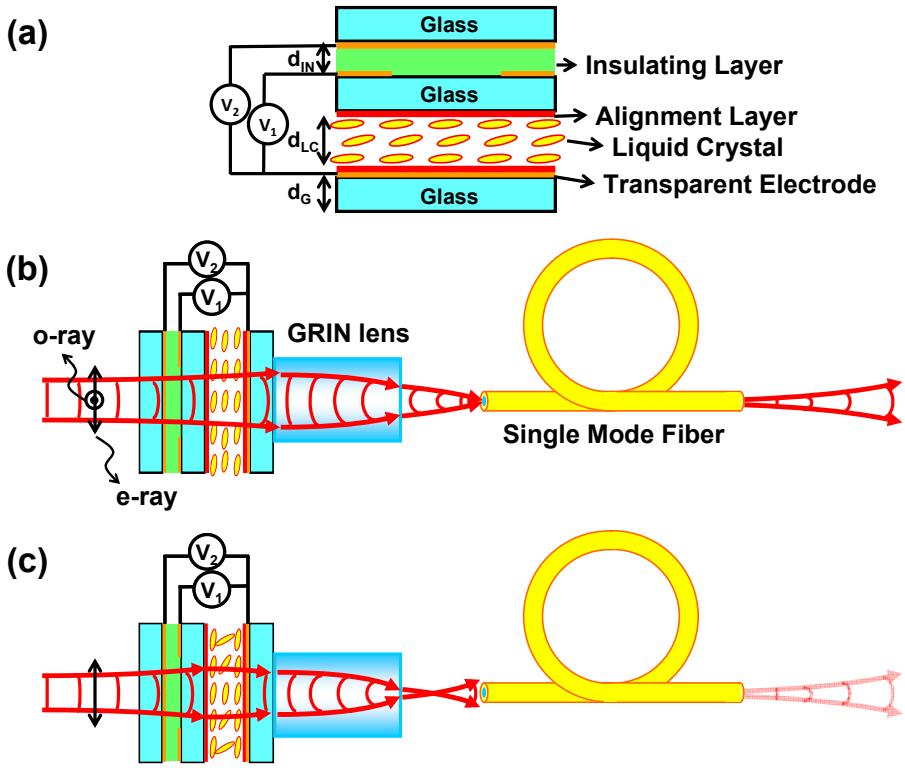

Figure 1. (a) The detailed structure of the LC lens shown in (b) and (c). (b) Wavefront for propagation of both e-ray and o-ray incident light as the lens power of the LC lens is zero. (c) Wavefront for propagation of e-ray when the LC lens provides a positive lens power. d_{IN}, d_{LC}, and d_G represent the thickness of distinct layer inside the LC lens.

Fig. 1 (b) and (c) illustrate the operating principle for fiber coupling, variable optical attenuation as well as polarization selection. An incident Gaussian beam first passes through the LC lens, propagates through a GRIN lens, and then impinges on a single mode fiber. When the voltages V_1 and V_2 are identical, the LC molecules have a single orientation. Both e-ray and o-ray, whose polarization are parallel and perpendicular to the alignment of the LC layer respectively, experience a homogeneous phase distribution and transmit through the LC lens without convergence or divergence. Hence, both e-ray and o-ray have the same wavefront and are converged by the GRIN lens. Because the distance between the GRIN lens and the fiber is designed to be the working distance of the GRIN lens, the beam waist appears at the entrance of the fiber, which results in a maximum coupling efficiency. At this moment, the tunable lens coupler works as a lens coupler, as depicted in Fig. 1(b). In Fig. 1(c), an e-ray incidents on the LC lens as V_1 is larger than V_2, where a positive lens power is provided by the LC layer under an inhomogeneous electric field distribution. Therefore, e-ray is first focused by the LC lens and then converged via the following GRIN lens. Under the circumstances, the focused beam waist appears slightly in front of the optical fiber. Increase of the beam size incident on the fiber with diverging wavefront thereafter causes a reduction of the coupling efficiency. This phenomenon becomes more obvious when the LC lens provides larger lens power. Consequently, the continuously increasing optical power attenuation inside the single mode fiber while increasing the lens power let the tunable lens coupler equip the function of VOA. Meanwhile, the o-ray, in contrast, sees a uniform phase distribution, which means the wavefront is barely changed as propagating through the LC lens. As a result, most of the incident light is converged via the GRIN lens and couple into

the fiber, just as that illustrated in Fig. 1 (b). Therefore, o-ray has a relatively high coupling efficiency while e-ray encounters a great power loss after transmitting through the fiber system. The polarization dependent transparency indicates that a linear polarizer can be achieved with the tunable lens coupler.

2.1 Theoretical analysis of the coupling coefficient

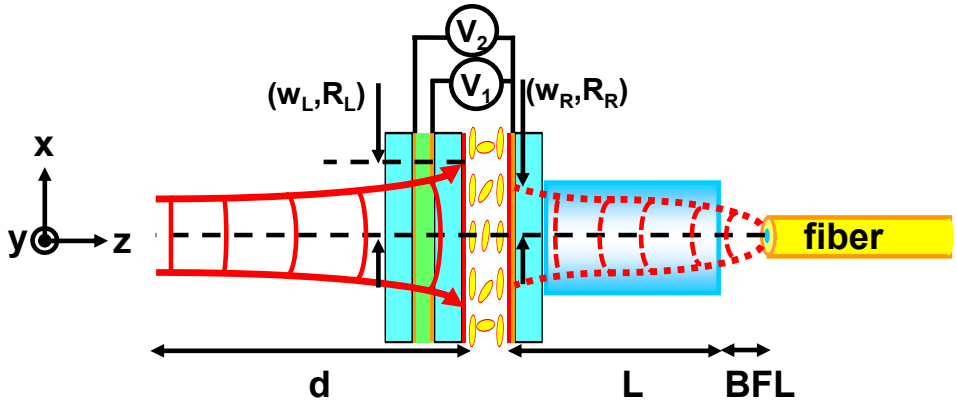

Figure 2. Schematic diagram for coupling efficiency evaluation of single mode fiber system with a tunable lens coupler

In order to calculate the coupling efficiency of a single mode fiber system shown in Fig. 2, several parameters need to be acquired. First of all is the beam size and radius of curvature of the incident beam, noted as w_L and R_L respectively because they are on the left side of the LC lens in Fig. 2. These parameters can be evaluated by means of the beam optics with a Gaussian beam propagating a distance (d) along z-direction, as shown with the solid red lines. On the other hand, similarly, we also have to know the beam size and radius of the curvature of the perfectly coupled beam, called w_R and R_R respectively because they are on the right side of the LC lens. To find these parameters, an imaginary Gaussian beam with its beam waist at the end of the fiber propagates from the fiber toward the LC lens. In addition, the beam waist is equal to the mode field radius of the single mode fiber. The beam propagates a back focal length (BFL) of the GRIN lens and transmits through the GRIN lens of length L, and the corresponding w_R as well as R_R can then be calculated. The last thing required is the lens power (P_{LC}) provided from the LC lens, which determines the phase distribution experienced by the incident beam. With the information above, the complex field of Gaussian beam expressions for the incident beam (Φ_L) and the perfectly coupled beam (Φ_R) can be written as the following,

$$\Phi_{L,R} = A_{L,R} \cdot \frac{1}{w_{L,R}} \cdot \exp\left(-\frac{x^2+y^2}{w_{L,R}^2}\right) \cdot \exp\left(-i \cdot \frac{k \cdot (x^2+y^2)}{2 \cdot R_{L,R}}\right) \quad (1)$$

where A represent a constant amplitude of the Gaussian beams, k is the wave number ($2\pi/\lambda$) which depends on the wavelength (λ) of the incident light. Moreover, the transmission function of the LC lens (T) can be expressed as the following, neglecting the scattering, other order aberration, and Fresnel reflection,

$$T(P_{LC}) = \exp\left(i \cdot \frac{\pi \cdot P_{LC} \cdot (x^2+y^2)}{\lambda}\right) \quad (2)$$

which is related to the wavelength of the incident light as well as the lens power generated by the LC lens. Therefore, the coupling efficiency (η) is thereafter obtained through overlap integral, using the Gaussian beams in Eq. (1) and transmission function of the LC lens. [18]

$$\eta = \frac{\left| \iint \Phi_L(x,y) \cdot T(x,y) \cdot \Phi_R^*(x,y) dxdy \right|^2}{\iint \left| \Phi_L(x,y) \right|^2 dxdy \cdot \iint \left| \Phi_R(x,y) \right|^2 dxdy} \tag{3}$$

Hence, with acquisition of information from the incident beam, optical fiber, and the LC lens, we can estimate the power transmittance of this fiber system. In addition, the coupling efficiency can be continuously manipulated when we adjust the wavefront by means of the LC lens.

3. SIMULATION, EXPERIMENT RESULTS AND DISCUSSION

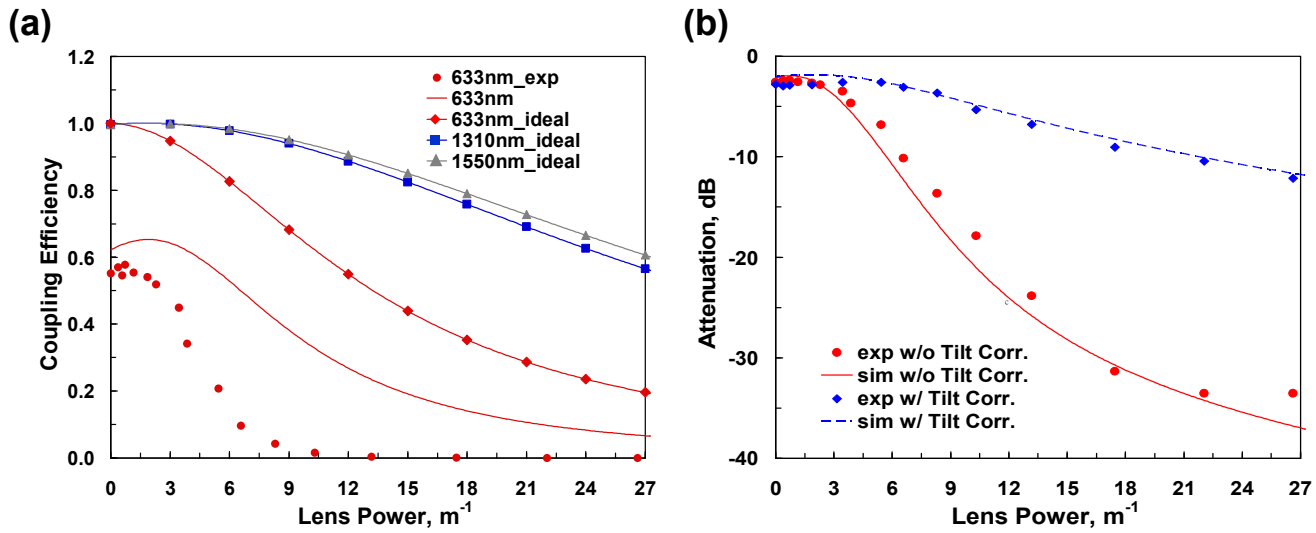

Figure 3. (a) Experimental and simulated coupling efficiency variation under different lens power for different incident wavelength. (b) Experimental and simulated optical attenuation under distinct lens power with and without tilt angle correction for incident wavelength λ= 633 nm.

In our experiment, a Gaussian beam with wavelength 633nm (Melles Griot, 05-srp-812), whose beam waist is 0.225 mm, propagates a distance of 28.5 cm until it impinges on the LC lens. In addition, a linear polarizer and a half-wave plate (HWP) are placed between the laser source and the LC lens, and the transmission axis of the polarizer and the fast axis of the HWP are parallel to the alignment direction of the LC molecules. After transmitting through the LC lens, the Gaussian beam is incident on a pigtail fiber (Thorlabs, 50-630-FC), which is attached with the LC lens and is composed of a GRIN lens and a single mode fiber. A power meter (OPHIR, AN/2) was placed at the other end of the fiber to detect the energy of output light. The central refractive index, gradient constant, length and the BFL of the GRIN lens are 1.6073, 0.339 mm^{-1}, 4.26 mm and 0.234 mm respectively, and the mode field diameter is 4.3 μm. Therefore, by using the physical properties of Gaussian beam, the corresponding w_L and w_R in Fig. 2 can be evaluated, which are 0.341 mm and 0.173 mm. Similarly, the reciprocal of the radius of curvature R_L and R_R are also calculated, which have values 0.002

mm^{-1} and 0 mm^{-1} respectively. Moreover, the LC lens we used can provide a tunable lens power range from 0 m^{-1} to 27m^{-1} for both visible light and near infrared light based on our previous measurement [16-17]. Hence, with the parameters mentioned above, we can find the theoretical values of coupling efficiency and optical attenuation as a function of lens power by using Eq. (1)-(3). In Fig. 3(a), red circles are the experimental results of coupling efficiency of the fiber system for wavelength 633nm under multiple lens powers provided via the LC lens. The corresponding theoretical values are also shown as a solid red line in Fig. 3(a). When the lens power is nearly equal to 0 m^{-1}, the coupling efficiency approaches its maximum, because the incident beam is mainly converged by the GRIN lens and the focused beam waist occurs at the entrance of the fiber, as shown in Fig. 1(b). At this moment, the tunable lens coupler has a function of lens coupler. As the lens power increases, the coupling efficiency decreases nearly monotonically. This is caused by the diverging wavefront and broadened beam waist incident on the fiber. The maximum coupling efficiency is ~0.6, which still suffers from a small optical loss due to the mismatch of Φ_L and Φ_R in Eq. (1). To achieve the ideal coupling condition, we can use a beam coming out of another pigtail fiber, which is exactly identical to that attached with the LC lens, as the incident light source. Under the circumstances, Φ_L and Φ_R can be nearly the same, resulting in a coupling efficiency close to 1. Theoretical coupling efficiencies for wavelengths 633nm, 1310nm, and 1550nm, is then calculated under the ideal coupling condition, which is represented by red line with diamonds, blue line with squares, and gray line with triangles, respectively. The mode field diameters for wavelengths 1310 nm and 1550 nm in our simulation are 9.2 μm and 10.4 μm, which are commonly used in single mode fibers (Corning, SMF-28) for optical communication. In addition, the dispersion of the GRIN lens is also considered. As we can observe in Fig. 3(a), the maximum coupling efficiency happens as the lens power is 0 m^{-1} for wavelength 633nm, while it occurs when the lens power is ~3 m^{-1} for the two infrared light. This means that we can always adjust the lens power of the LC lens to achieve the maximum coupling condition for light with a wide spectrum range, which results in a broad band lens coupler. On the other hand, the optical attenuation can be expressed by showing coupling efficiency in decibel. In Fig. 3(b), the red circles and the blue dashed lines are experimental and simulation results of optical attenuation, which is exactly the same data set as the red circles and the red line in Fig. 3(a) respectively. There exists an obvious difference that the maximum attenuation in our experiment is far larger than that expected in the blue dashed line. The main reason is that the beam is somehow tilted after it passes through the LC lens. Hence, at each lens power, we mechanically adjust the tilt angle of the GRIN lens with respect to the z-direction in Fig. 2 until the minimum attenuation occurs, as indicated by the blue diamonds in Fig. 3(b). With tilt angle correction, the experimental results are nearly identical to the theoretical values. On the other hand, when we take the tilt angle into count and modify the overlap integral in Eq. (3), the simulation for the tilted beam can also be conducted, and the corresponding values are shown as the red line in Fig. 3(b). The calculation shows a similar result as the experimental data without tilt angle correction. The origin of the tilted beam as well as detail for the modified equation will be discussed in the next paragraph. In Fig. 3(b), the attenuation becomes larger as we increase the lens power and the tunable range is up to 30 dB. This indicates that the tunable lens coupler is capable to continuously control the optical loss in the fiber system, which has a function of VOA.

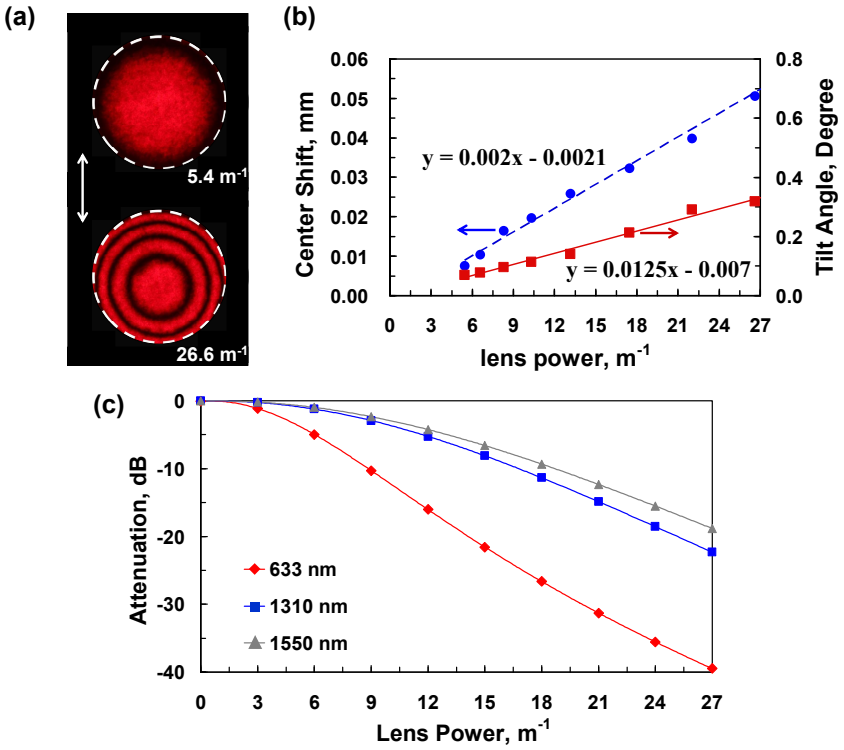

Figure 4. (a) Phase profiles of the LC lens for wavelength 633 nm when the lens power is 5.4 m^{-1} and 26.6 m^{-1}. The white dashed circle indicates a 0.72 mm region at the center of the hole-pattern and the white arrow shows the alignment direction of the LC lens. (b) The center shift of the phase profile and the corresponding tilt angle of the incident beam versus lens power. (c) Theoretical simulation of optical attenuation under ideal coupling condition for 3 different operational wavelengthes 633 nm, 1310 nm, and 1550 nm.

To quantify the tilt angle of the incident beam, we observed the phase profiles of the LC lens under crossed-polarizers with the alignment of the LC molecules at 45 degree with the two transmission axes [16-17]. As we can see in Fig. 4(a), a central region with 0.72 mm diameter is circled by white dashed lines, and the center of the parabolic phase profile has a displacement from the center of the hole-pattern on the ITO electrode. In addition, the displacement becomes larger as the lens power increases. This center shift of the parabolic phase is originated from the pretilt angle of the LC molecules between the alignment layers. While the LC layer with a pretilt angle is applied a circularly symmetric non-uniform electric field [19], appearing in the LC lens structure in Fig. 1(a), the rotation of LC molecules would not be symmetric along the alignment direction. As a result, the LC molecules rotate more on the top half of the phase profiles and less on the bottom half in Fig. 4(a). The incident beam is then not only converged but also bent by the LC lens as transmitting through the LC layer due to off axis incidence. In Fig. 4(b), the corresponding center shift between the center of the parabolic phase distribution and the center of the hole-pattern is shown as blue circles. Moreover, a linear blue dashed line indicates the least square fitting of the center shift. In our observation, the center shift increases almost linearly as we enlarge the lens power. The tilt angle of the Gaussian beam after propagating through the LC lens can be approximately evaluated as $\frac{\lambda \cdot N}{D_{eff}}$ [20], where λ is the operational wavelength, and N and D_{eff} are the number of bright lines and

distance between the center of the parabolic phase and the top edge of the white dashed circle. As depicted in Fig. 4 (b), the red squares are the tilt angles under different lens power, and a linear fitting red line is also provided. Therefore, we can modify the overlap integral and evaluate the theoretical value with the following formula, [18]

$$\eta' \approx \frac{\left| \iint \Phi_L(x' \cdot \cos\theta, y') \cdot T(x' \cdot \cos\theta - x_s, y') \cdot \Phi_R^*(x', y') dx' dy' \right|^2}{\iint |\Phi_L(x' \cdot \cos\theta, y')|^2 dxdy \cdot \iint |\Phi_R(x', y')|^2 dxdy} \tag{4}$$

where θ represents the tilt angle of the incident beam and x_s is the amount of center shift under different lens power. The theoretical result shown in Fig. 3(b) coincides with the experimental data and indicates the critical influence on the attenuation caused by a small beam tilting. As for the optical loss of the ideal coupling condition, those in Fig. 3(a), with the beam bending effect, we also find the tunable range for wavelengths 633 nm, 1310 nm, and 1550 nm by means of Eq. (1)-(2) and Eq. (4). When the lens power is equal to zero, the coupling efficiency approaches its maximum value ~1 because of the perfect match of $w_L(R_L)$ and $w_R(R_R)$. At this moment, the LC lens barely affects the incident light. As the lens power starts to increase, the attenuation at three wavelengths grows monotonically due to the converging and bending effect caused by the LC lens. Optical power has a minimum transmittance through this fiber system while the lens power reaches its maximum (27 m^{-1}) for all the wavelengths. Different capability of controlling the attenuation for different operational wavelength is mainly caused by the Gaussian beam characteristics as well as distinct mode field diameters. Hence, the tunable lens coupler can continuously manipulate the optical loss and the tunable range for 633nm, 1310 nm, and 1550 nm are 39 dB, 22 dB, and 19 dB, which let it become a nice candidate for VOA in fiber communication systems.

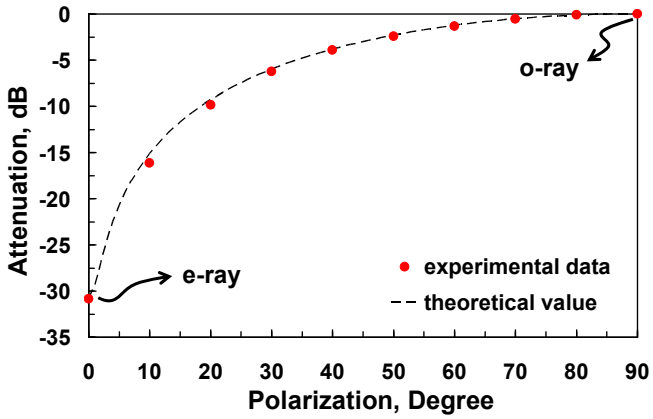

Figure 5. Experimental and theoretical optical attenuation for incident light with different polarization. The operational wavelength is 633 nm and the polarization is expressed in angle between the polarization direction and the alignment direction of the LC layer.

In order to measure the influence of the polarization on the optical attenuation, we rotated the HWP between the linear polarizer and the LC lens, and the variation of the output power was recorded at distinct polarization state when the lens power is equal to ~27 m^{-1}. Therefore, the polarization direction of the incident beam rotated without changing its optical power, and still remained linear polarized. In addition, the rotation angle was two times the angle between the alignment

direction and the fast axis of the HWP. When the polarization is parallel to the alignment direction of the LC molecules, all the incident light is composed of e-ray, noted as 0 degree. As the polarization is perpendicular to the alignment of the LC layer, the incident light contains only o-ray, which is noted as 90 degree. The relative attenuation obtained in the experiment compared to the attenuation of o-ray is marked as red circle in Fig. 5. Moreover, under the assumption that LC layer is analogical to a uni-axial crystal, the theoretical values can also be evaluated, as the black dashed line shown in Fig. 5. e-ray experienced an inhomogeneous phase distribution provided by the LC lens, while o-ray saw a homogeneous index of refraction as propagating through the LC layer. Hence, most of the o-ray was coupled into the fiber and e-ray encountered a huge optical loss, as illustrated in Fig. 1(b)-(c). The larger the polarization angle was, the lower the optical loss became, because the ratio of o-ray to e-ray increased. As a consequence, there exists a large difference of attenuation between e-ray and o-ray, which is defined as polarization dependent loss (PDL). The ability of such polarization selection makes our tunable lens coupler a polarizer for single mode fiber systems, whose PDL is up to ~30 dB. Similarly, this can be applied to incident light with infrared wavelength.

To further increases the tunable range of lens power of the tunable lens coupler, the diameter of the hole-pattern should be reduced, which allows LC lens to generate a higher gradient of refractive index. Besides, a LC with higher birefringence in infrared region needs to be used for practical application. Recently, combination of a thin passive lens, composed of liquid crystal and polymer composite film, and active LC layer has been demonstrated [21], and a multi-layer liquid crystal lens technology was also proposed [15]. As a result, it is possible to replace the GRIN lens in present device with multi-layer polymer composite films. This can largely reduce the size of the tunable lens coupler, and make it more compatible with small scale photonics systems.

4. CONCLUSION

We demonstrated an electrically tunable lens coupler adopting an LC lens, which has a combination of multiple function, including fiber coupling, optical power attenuation, and polarization selection. Before an external electric field is applied on the LC lens, the incident beam experiences a homogeneous phase distribution inside the LC layer and it is only converged by a GRIN lens. Hence, most of the light is coupled in to a single mode fiber, resulting in high coupling efficiency. Under the circumstances, the tunable lens coupler acts as a conventional lens coupler. As a lens power is provided from the LC lens, the wavefront of the incident beam is thereafter altered, which reduces the coupling efficiency and increases optical attenuation. In addition, a slightly shift of the LC lens due to pretilt of LC molecules induces a bent of the incident light, which largely decreases the transmitting optical power in the fiber system. Therefore, a function of VOA is then demonstrated for a wide spectrum range. Besides, the e-ray has a huge optical attenuation while the o-ray remains coupled into the fiber because of the anisotropic property of the LC lens. Consequently, a polarizer for single mode fiber system can also be achieved. We believe this study provides new opportunities for multi-functional photonic devices applying in ubiquitous fiber communication systems nowadays.

REFERENCES

[1] Woltman, S. J., Crawford, G. P., and Jay, G. D., [Liquid Crystals: Frontiers in Biomedical Applications], Hackensack, NJ, USA: World Scientific, (2007).

[2] Lin, Y. H., Chu, T. Y., Chu, W. L., Tsou, Y. S., Chiu, Y. P., Lu, F., Tsai, W. C., and Wu, S. T., "A sperm testing device on a liquid crystal and polymer composite film," J. Nanomedicine Nanotechnol. S9(001), 1-5 (2011).

[3] Lin, Y. H., Chang, K. H., Chu, W. L., Tsou, Y. S., Wu, L. C., and Li, C. F., "A biosensor of high-density lipoprotein of human serum on a liquid crystal and polymer composite film," Proc. SPIE 8828, 88280I (2013).

[4] Hirabayashi, K., Wada, M., and Amano, C., "Optical-fiber variable-attenuator arrays using polymer-network liquid crystal," IEEE Photon. Technol. Lett. 13(5), 487–489 (2001).

[5] Wu, Y. H., Liang, X., Lu, Y. Q., Du, F., Lin, Y. H., and Wu, S. T., "Variable optical attenuator with a polymer-stabilized dual-frequency liquid crystal," Appl. Opt. 44(20), 4394–4397 (2005).

[6] Sato, S., "Liquid-crystal lens-cells with variable focal length," Jpn. J. Appl. Phys. 18(9), 1679–1684 (1979).

[7] Ren, H., and Wu, S. T., [Introduction to Adaptive Lenses], Hoboken, NJ, USA: Wiley, (2012).

[8] Feng, J., Zhao, Y., Li, S. S., Lin, X. W., Xu, F., and Lu, Y. Q., "Fiber-optic pressure sensor based on tunable liquid crystal technology," IEEE Photon. J. 2(3), 292–298 (2010).

[9] Brasselet, E., Murazawa, N., Misawa, H., and Juodkazis, S., "Optical vortices from liquid crystal droplets," Phys. Rev. Lett. 103(10), 103903 (2009).

[10] Wei, B. Y., Hu, W., Ming, Y., Xu, F., Rubin, S., Wang, J. G., Chigrinov, V., and Lu, Y. Q., "Generating switchable and reconfigurable optical vortices via photopatterning of liquid crystals," Adv. Mater. 26(10), 1590–1595 (2014).

[11] Lin, H. C., and Lin, Y. H., "A fast response and large electrically tunable-focusing imaging system based on switching of two modes of a liquid crystal lens," Appl. Phys. Lett. 97(6), 063505 - 063505-3 (2010).

[12] Chen, M. S., Chen, P. J., Chen, M., and Lin, Y. H., "An electrically tunable imaging system with separable focus and zoom functions using composite liquid crystal lenses," Opt. Express 22(10), 11427-11435 (2014).

[13] Tsou, Y. S., Lin, Y. H., and Wei, A. C., "Concentrating photovoltaic system using a liquid crystal lens," IEEE Photon. Technol. Lett. 24(24), 2239-2242 (2012).

[14] Chen, M. S., Collings, N., Lin, H. C., and Lin, Y. H., "A holographic projection system with an electrically adjustable optical zoom and a fixed location of zeroth-order diffraction," Opt. Express 20(25), 27222-27229 (2014).

[15] Lin, Y. H., and Chen, H. S., "Electrically tunable-focusing and polarizer-free liquid crystal lenses for ophthalmic applications," Opt. Express 21(8), 9428-9436 (2013).

[16] Chen, M., Chen, C. H., Lai, Y. C., and Lin, Y. H., "An electrically tunable liquid crystal lens for fiber coupling and variable optical attenuation," J. Electr. Electron. Syst. 3(2), 1-5 (2014).

[17] Chen, M., Chen, C. H., Lai, Y. C., Lu, Y. Q., and Lin, Y. H., "An electrically tunable polarizer for a fiber system based on a polarization-dependent beam size derived from a liquid crystal lens," IEEE Photon. J. 6(3), 7100408 (2014).

[18] Yuan, S., and Riza, N. A., "General formula for coupling-loss characterization of single-mode fiber collimators by use of gradient-index rod lenses," Appl. Opt. 38(15), 3214-3222 (1999).

[19] Ye, M., Wang, B., and Sato, S., "Liquid-crystal lens with a focal length that is variable in a wide range," Appl. Opt. 43(35), 6407-6412 (1999).

[20] Riza, N. A., and Khan, S. A., "Liquid-crystal-deflector based variable fiber-optic attenuator," Appl. Opt. 43(17), 3449-3455 (2004).

[21] Lin, H. C., and Lin, Y. H., “An electrically tunable-focusing liquid crystal lens with a built-in planar polymeric lens” Appl. Phys. lett. 98, 083503 (2011).